ACS APPLIED NANO MATERIALS

www.acsanm.org Article

Ru(II) Polypyridyl-Modified TiO_2 Nanoparticles for Photocatalytic C−C/C−O Bond Cleavage at Room Temperature

Shuya Li,[#] Udani K. Wijethunga,[#] Andrew H. Davis, Saerona Kim, Weiwei Zheng, Benjamin D. Sherman, Chang Geun Yoo, and Gyu Leem*

Cite This: *ACS Appl. Nano Mater.* 2022, 5, 948−956 Read Online

ACCESS | Metrics & More | Article Recommendations | Supporting Information

ABSTRACT: Bond cleavage reactions including that of C−C and C−O bonds are important to the chemical industry and organic chemistry. Performing this chemical transformation under mild conditions (e.g., room temperature, solar light) can benefit both the selectivity and yield of the targeted products. This manuscript describes a simple one-pot approach used to carry out C_α−C_β/C_β−O σ-bond cleavage using photocatalytic nanoparticles that afford the cleavage products in excellent yields at room temperature with visible-light illumination. We synthesized a carboxylic acid-functionalized Ru^{II} polypyridyl complex (RuC) and TiO_2 nanoparticles (TiO_2 NPs) with the average dimensions of 6.6 nm width and 14.7 nm length using a hydrothermal method. The photocatalyst RuC was immobilized onto TiO_2 NPs (RuC-TiO_2 NPs) to perform a photocatalytic cleavage reaction with a nonphenolic lignin model compound, 1-(3,4-dimethoxyphenyl)-2-(2-methoxyphenoxy)propane-1,3-diol (DMP-2ol), under simulated solar illumination. Photophysical studies of RuC and TiO_2 NPs reveal that intermolecular energy/electron transfer from the photoexcited RuC to TiO_2 NPs occurs in acetonitrile solution. Under ambient temperature and aerobic conditions, the photocatalytic reaction with RuC-TiO_2 NPs and DMP-2ol generates the main C_α−C_β/C_β−O bond cleavage products of 3,4-dimethoxybenzaldehyde (**1**, 82%) and 2-methoxyphenol (**2**, 90%) in excellent yields. This study successfully performed the C−C/C−O bond cleavage reaction using a homogeneously dispersed photocatalytic system at room temperature, under solar illumination, and without the need for additional mediators or oxidizing/reducing agents. This system presents a possible approach to support light-driven lignin depolymerization under mild conditions, which is a target of future work.

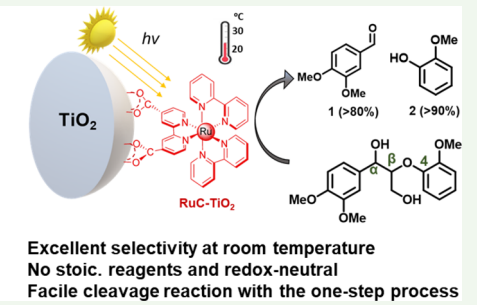

KEYWORDS: *ruthenium(II) polypyridyl chromophores, TiO_2 nanoparticles, bond cleavage, lignin degradation, heterogeneous photocatalysis*

INTRODUCTION

The selective cleavage of chemical bonds is crucial for various applications such as organic synthesis and depolymerization.[1,2] This chemical transformation, especially if carried out under mild conditions, is essential to making the degradation of lignin, a renewable alternative source to petroleum-based chemicals.[2−5] However, traditional lignin depolymerization processes that perform C−O/C−C bond cleavage require severe reaction conditions (e.g., high temperature and pressure) and result in poor selectivity and/or low productivity for producing targeted value-added aromatic chemicals.[2,6] Recent studies have focused on targeting C−C/C−O bond cleavage specifically to the β-aryl ether repeating motifs found in lignin, and the use of structural model compounds has led to the formation of well-defined aromatic chemicals.[4,7−12] Recently, a two-step C−C/C−O bond cleavage strategy was reported using β-O-4 lignin models with the first step in the process involving the oxidation of the C_α−OH.[9,13,14] The homolytic C_β−O bond dissociation energy in the β-O-4 linkage decreases from 69.2 to 55.9 kcal/mol after oxidation of the C_α−OH to give the C_α═O.[7] Then, the C_α═O in the lignin facilitates the reductive cleavage of the C_β−O bond. In 2020, our group developed a hydrogen atom transfer mediator (HAT) coupled TiO_2-based photoanode for the photocatalytic cleavage of the C−C bond or oxidation of the C_α−OH in lignin models under mild conditions.[15,16] This photoelectrochemical heterogeneous catalytic process exhibited excellent conversion efficiencies (>90%) to the conversion of the oxidized ketone products from lignin models under visible-light illumination as a first step toward performing chemoselective C−O bond cleavage in lignin.[15] This previous study showed that interfacial oxidation of lignin models at the surface-bound Ru(II)-sensitized mesoporous TiO_2 film offers a promising chemical strategy for C−C/C−O bond cleavage in the presence of the nitroxyl radical species. However, the

Received: October 28, 2021
Accepted: December 21, 2021
Published: December 30, 2021

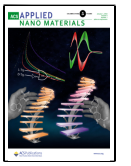

effectiveness of polypyridyl metal complex-immobilized TiO_2 NPs for performing the bond cleavage reaction in the absence of the nitroxyl radical species has not been studied in colloidal nanoparticulate systems. Thus, investigating metal chromophore-sensitized TiO_2 nanoparticles for carrying out $C_\alpha-C_\beta/C_\beta-O$ bond cleavage is the focus of this study.

The photocatalytic conversion of lignin to small aromatic products has been studied using ultraviolet (UV) illumination and TiO_2 NPs because TiO_2 NPs generate strong oxidizing equivalents, are inexpensive to synthesize, and have good chemical stability.[17−19] For example, Wang and co-workers reported the photocatalytic cleavage of the C−O bond of β-O-4 ketones selectively in lignin model compounds using TiO_2 under UV illumination (e.g., λ < 365 nm) via a tandem oxidation−hydrogenolysis reaction under mild conditions.[20] Ti^{3+} from TiO_2 photocatalysts can activate the C−O bonds under UV-light illumination. Due to its high band gap ($E_g \approx$ 3.2 eV, anatase TiO_2) and the short diffusion length of photoinduced excitons, it needs to develop an effective way to extend the absorbance of TiO_2 toward the visible region.[21] Ru(II) polypyridyl complexes under irradiation by visible light with λ > 400 nm are widely used as an effective visible-light sensitizer for TiO_2 because of their chemical stability and excited-state reactivity.[22,23] This study proves that TiO_2 NPs modified with carboxylic acid-functionalized bis(2,2′-bipyridine)(4,4′-dicarboxy-2,2′-bipyridine)Ru(II) (RuC) can be utilized for the C−O/C−C bond transformation in the lignin model compound under visible or solar light illumination.

According to previous studies, cleavage products **1** and **2** formed from the methoxy-substituted nonphenolic lignin model compound, 1-(3,4-dimethoxyphenyl)-2-(2-methoxyphenoxy)propane-1,3-diol (DMP-2ol), can be obtained by thermal or visible-light oxidative cleavage reactions with metal-based homogeneous catalysts as shown in Figure 1.[24,25] For example, under a high temperature (e.g., 100 °C), **1** and **2** were obtained in 46 and 47% yields using $FeCl_3$-derived iron catalysts with an oxidizing agent.[24] Instead of this harsh condition, Mitchell and Moody reported the visible-light-driven cleavage affording products **1** (∼18%) and **2** (∼8%) using Cu nanoparticles in the presence of 1,4-benzoquinone and O_2 at room temperature.[25] This oxidative cleavage reaction required both an oxidizing agent and O_2. Importantly, due to mild conditions (room temperature), the product yield was not as high as that observed with the Fe^{3+} catalyst at 100 °C. Very recently, we reported the oxidative cleavage of a phenolic lignin model compound at room temperature at a photoanode with a HAT co-catalyst in solution, specifically, 4-acetamido-2,2,6,6-tetramethyl-1-peperidine-*N*-oxyl (ACT). In the oxidized (oxoammonium) form, ACT serves as a hydrogen transfer mediator for the cleavage of the $C_{aryl}-C_\alpha$ bond in lignin model compounds.[15] This DSPEC system requires the ACT mediator to activate HAT catalysis, leading to oxidative cleavage. Our previous study explored the photocatalytic cleavage reaction with phenolic and nonphenolic lignin model compounds in the DSPEC.[15] We observed that the phenolic lignin model compound underwent C−C bond cleavage with high efficiency in a dye-sensitized photoelectrochemical cell. However, C−C and/or C−O bond cleavage did not occur, but benzylic alcohol oxidation from $C_\alpha-OH$ to $C_\alpha=O$ was observed in a nonphenolic lignin model compound.

This manuscript presents the use of TiO_2 NPs with surface-bound carboxylic acid-functionalized Ru^{II} polypyridyl complexes to perform solar-light-driven cleavage of $C_\alpha-C_\beta/C_\beta-O$ bonds in a nonphenolic lignin model compound as shown in Figure 1. Our current study is focused on the photocatalytic cleavage reaction with a nonphenolic lignin model, DMP-2ol. RuC was used with TiO_2 NPs because of (1) the proper redox potential with the conduction band of TiO_2, (2) a strong metal-to-ligand charge transfer (MLCT) transition in the visible region, and (3) the presence of anchoring moieties covalently immobilized to the surface of metal oxide.[22,26−29] The RuC-anchored TiO_2 nanoparticles (RuC-TiO_2 NPs) used in this study are found to cleave the $C_\alpha-C_\beta/C_\beta-O$ σ-bonds in the β-aryl ether linkage in lignin materials. Two major products (**1** and **2**) were found after simulated solar illumination at room temperature, while no products were found for the unmodified TiO_2 NPs. This current study presents a facile method to cleave $C_\alpha-C_\beta/C_\beta-O$ σ-bonds in excellent yield without the need of mediators or stoichiometric oxidizing/reducing agents at room temperature.

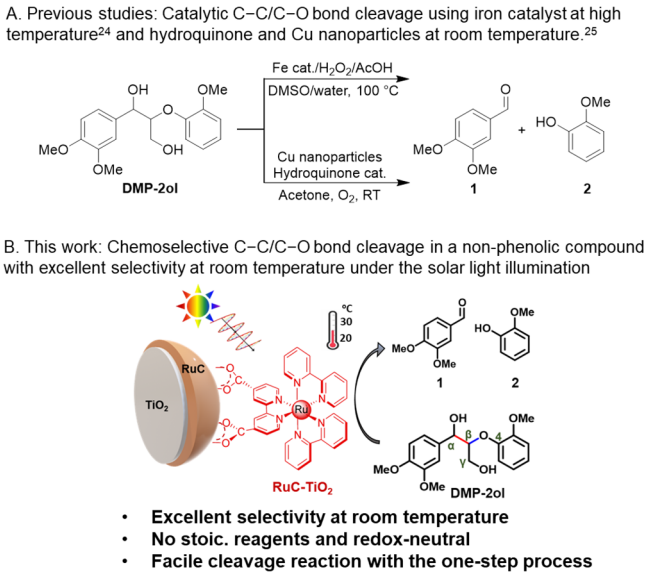

Figure 1. (a) Examples of catalytic $C_\alpha-C_\beta/C_\beta-O$ bond cleavage strategies with a methoxy-derivatized nonphenolic lignin model compound.[24,25] (b) Structures of the corresponding nonphenolic lignin model, 1-(3,4-dimethoxyphenyl)-2-(2-methoxyphenoxy)-propane-1,3-diol (DMP-2ol), cleavage products **1** and **2**, and schematic illustrating the carboxylic acid-functionalized RuC-immobilized TiO_2 NPs and photocatalytic $C_\alpha-C_\beta/C_\beta-O$ cleavage reaction of DMP-2ol via a one-pot process under solar light illumination at room temperature.

RESULTS AND DISCUSSION

To investigate the crystalline phase structure of the bare TiO_2 NPs and RuC-TiO_2 NPs, X-ray diffraction (XRD) characterizations were carried out at room temperature (Figure 2a). All of the crystalline structures of the TiO_2 NPs and RuC-TiO_2 NPs indicate the anatase TiO_2 phases with similar diffraction patterns according to JCPDS file 21-1272.[30] The XRD pattern of RuC-sensitized TiO_2 NPs did not exhibit additional diffraction peaks, indicating that the TiO_2 anatase nature was unchanged.[21] Interestingly, the crystallite XRD sizes for bare TiO_2 NPs and RuC-TiO_2 NPs were 5.6 and 6.6 nm, respectively, which were obtained by applying the Debye−Scherrer equation of the (101) diffraction peak. The particle size and morphology of RuC-TiO_2 NPs were determined by

https://doi.org/10.1021/acsanm.1c03622
ACS Appl. Nano Mater. 2022, 5, 948−956

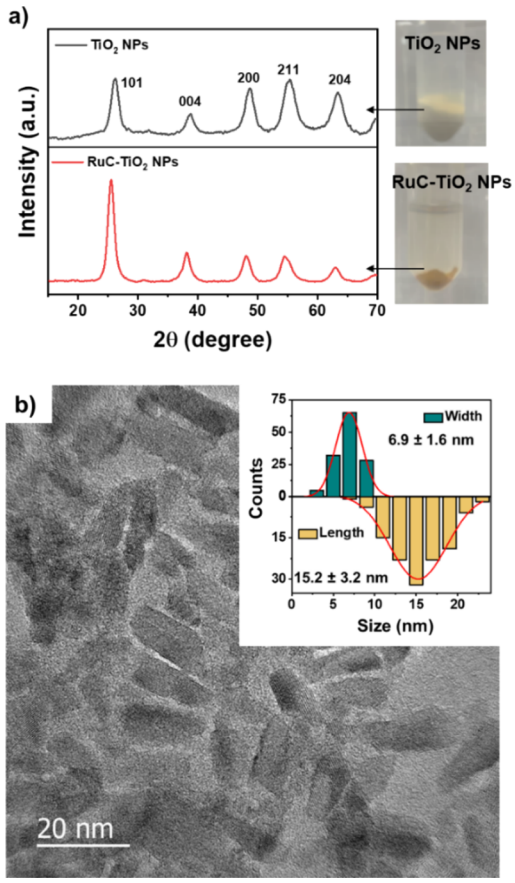

Figure 2. (a) Powder XRD diffraction patterns of (top) TiO_2 and (bottom) RuC-TiO_2 NPs. (b) TEM image of RuC-TiO_2 NPs. Scale bar = 20 nm. Inset: size distribution of RuC-TiO_2 NPs with the size of width and length.

TEM (Figure 2b). The RuC-TiO_2 NPs exhibit a nonuniform size distribution; the average size of approximately 6.9 nm width by 15.2 nm length is roughly similar to the average size of 6.6 nm width by 14.7 nm length of the bare TiO_2 NPs (Figure S1). Thus, the particle sizes of the TiO_2 NPs and RuC-TiO_2 NPs are not significantly different within the standard deviation.

Figure 3 shows the UV−Vis absorption and steady-state emission spectra of TiO_2 NPs and RuC-TiO_2 NPs in acetonitrile (ACN) solution. As shown in Figure 3a, the UV−Vis absorption spectrum of RuC-TiO_2 NPs indicates a strong $d\pi(Ru) \rightarrow \pi^*$(bipyridine, bpy) MLCT absorption band at $\lambda_{max} \approx 453$ nm, which is consistent with the MLCT absorption band at $\lambda_{max} \approx 460$ nm from RuC in ACN in the visible region (Figure S2). This slight change is related to the formation of a surface complex between RuC and the colloidal TiO_2 NPs.[31] Bare TiO_2 NPs display no obvious absorption in the visible range. In Figure 3b, the emission maxima of RuC and RuC-TiO_2 NPs in ACN exhibit intense photoluminescence at $\lambda_{max} \approx 642$ and 615 nm, respectively, from the MLCT excited state. The emission maximum from the RuC-TiO_2 NPs shows a 27 nm blueshift compared with the solvated RuC. From our earlier study, immobilization of RuC onto a TiO_2 nanorod film also showed a blueshift in emission.[15] We assume that this spectral shift can be explained by the aggregation of RuC complexes on the surface of the TiO_2 NPs[32,33] or intramolecular charge transfer emission from RuC*.[34]

To compare the band gap energy (E_g) of TiO_2 before and after the immobilization of RuC, Tauc plots of the bare TiO_2 NPs and the TiO_2 component extracted from the RuC-TiO_2 NP spectrum are shown in Figure 4. Tauc plots show an estimate of the E_g of TiO_2.[35] Figure 4b shows the Tauc plot of the TiO_2 spectra obtained by subtracting the RuC component from the RuC-TiO_2 spectra. The E_g values of TiO_2 measured for the bare TiO_2 NPs and RuC-TiO_2 NPs are 3.85 and 3.94 eV, respectively. It is interesting to note that the E_g (3.85 eV) of TiO_2 NPs increased in comparison with anatase-phase TiO_2 (3.20 eV), indicating the small size of TiO_2 NPs due to the quantum confinement effect in nanomaterials.[36,37] Thus, we conclude that the RuC coating onto the surface of the TiO_2 NPs does not affect the E_g of TiO_2 based on the Tauc plot data.

To understand the intramolecular energy/electron transfer from photoexcited RuC* to TiO_2 NPs, emission quenching and lifetime measurements of RuC with or without unmodified TiO_2 NPs were performed in ACN solution under argon. Note that the RuC was not preassembled on the TiO_2 NP surface in these experiments; rather, the emission of dissolved RuC* was monitored with increasing amounts of bare TiO_2 NPs added to solution. As shown in Figure 5a, emission from RuC* was slightly quenched by unmodified TiO_2 NPs ranging from 0 to 17.9 nM of TiO_2 NPs with an increment of 0.02 mg of TiO_2 per 1 mL in ACN solution. The molar quantity of TiO_2 NPs in ACN solution can be calculated according to a previous study.[38] We assume that the TiO_2 NPs possess a spherical

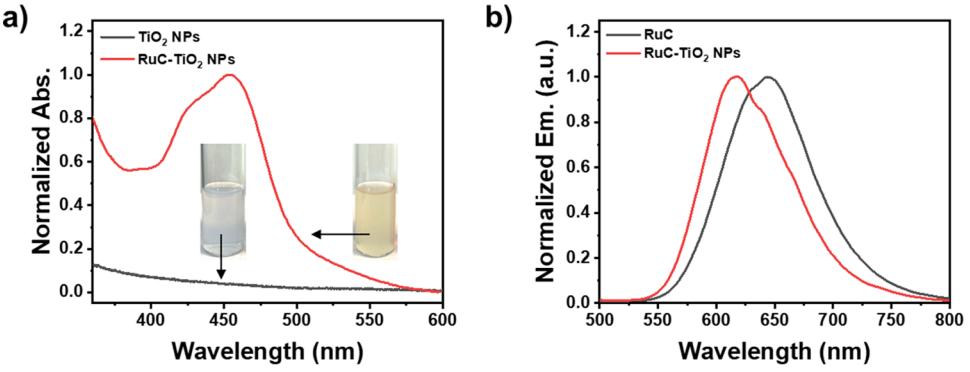

Figure 3. (a) Absorption spectra of colloidal TiO_2 NPs (black) and colloidal RuC-TiO_2 NPs (red) in ACN. The absorption spectrum of RuC-TiO_2 NPs in ACN was normalized to the λ_{max} value. Inset: pictures of colloidal TiO_2 NPs and RuC-TiO_2 NPs. (b) Emission spectra for RuC (black) and RuC-TiO_2 NPs (red) in ACN solution at room temperature upon photoexcitation at λ_{ex} = 450 nm.

https://doi.org/10.1021/acsanm.1c03622
ACS Appl. Nano Mater. 2022, 5, 948−956

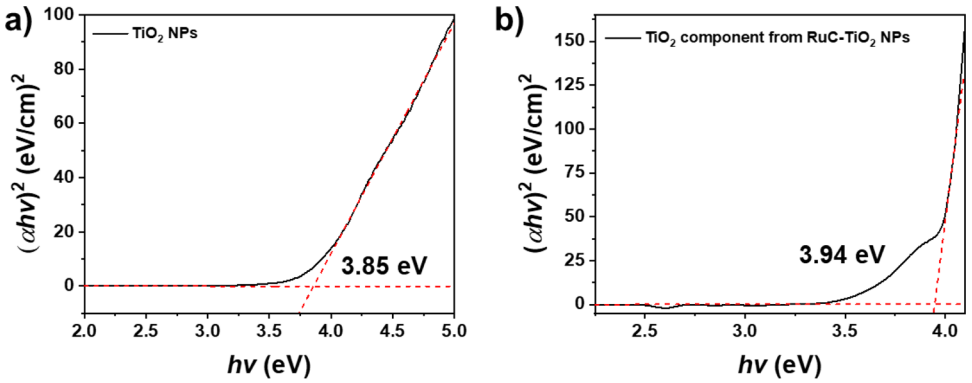

Figure 4. Tauc plots of (a) the bare TiO_2 NPs and (b) the TiO_2 component extracted from the RuC-TiO_2 NP spectrum. The estimated E_g values for bare TiO_2 NPs and RuC-TiO_2 NPs are shown by the *x*-axis intersection of the linear fit of the Tauc plots.

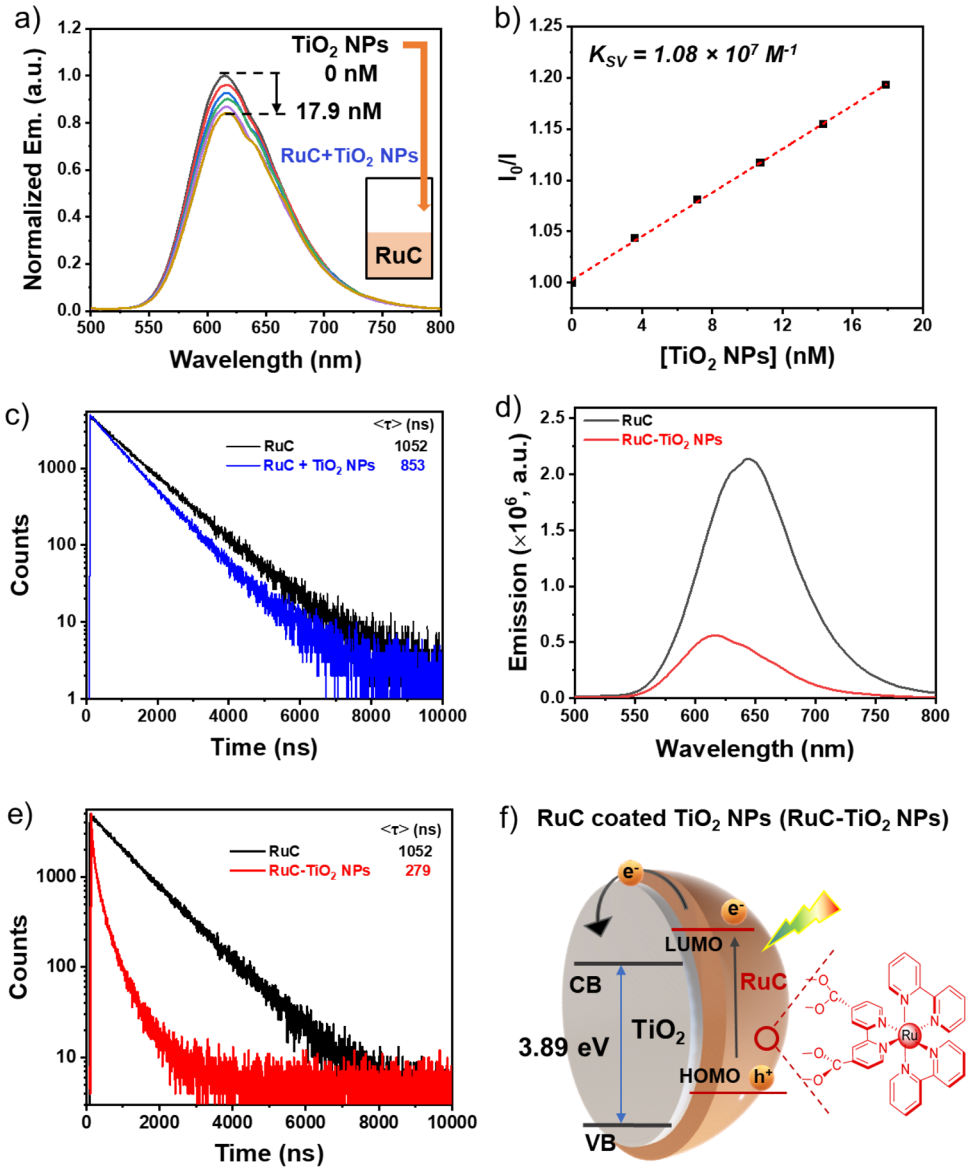

Figure 5. (a) Steady-state photoluminescence of RuC (0.014 mM) in the absence and presence of TiO_2 NPs in the concentration range of 0, 3.58 (0.02 mg/1 mL), 7.16 (0.04 mg/1 mL), 10.74 (0.06 mg/1 mL), 14.32 (0.08 mg/1 mL), and 17.9 (0.1 mg/1 mL) nM. (b) Stern−Volmer plots (I_0/I vs [Q], Q: TiO_2 NPs) for emission quenching of RuC by monitoring the emission intensity at 615 nm (λ_{ex} = 450 nm). (c) Comparison of emission lifetimes of RuC and RuC with 17.9 nM TiO_2 NPs. (d) Steady-state photoluminescence of RuC and RuC-TiO_2 NPs in ACN. (e) Emission lifetimes of RuC and RuC-TiO_2 NPs. (f) Energy diagram indicating the photoexcitation of surface-bound RuC to the conduction band of TiO_2 and the following energy transfer between TiO_2 NPs and excited-state RuC* (CB: conduction band, VB: valence band).

https://doi.org/10.1021/acsanm.1c03622
ACS Appl. Nano Mater. 2022, 5, 948−956

shape with a diagonal size of 16.1 nm calculated by the average size of width and length of TiO_2 NPs to determine the mass of the unit quantity of one particle. The molar concentration of the TiO_2 NPs can be calculated according to eq 1

$$c = \frac{N}{N_A V} \quad (1)$$

where c is the concentration, N_A is the Avogadro constant, N is the number of TiO_2 NPs in ACN solution, and V is the volume of the colloidal ACN solution. Figure 5b illustrates the Stern−Volmer plot of RuC with TiO_2 NP solution. The quenching constant value (K_{SV}) is approximately 1.08×10^7 M^{-1}. Figure 5c shows that the average emission lifetimes for RuC* with and without the TiO_2 NPs were 1052 and 853 ns, respectively, in ACN solution at room temperature. The emission lifetime of RuC* in the presence of TiO_2 NPs decreased by approximately 19%, which is consistent with the above emission quenching experiments. The decrease in fluorescence emission and lifetimes can be attributed to electron and/or energy transfer processes.[22,23,31] This observation suggests charge transfer from RuC* to the conduction band of TiO_2 NPs. To confirm the electron transfer from the surface-bound RuC to TiO_2, quenching and fluorescence lifetime measurements were performed with RuC-TiO_2 NPs in ACN; in this case, the RuC was pre-immobilized on the TiO_2 NP surface. Figure 5d shows that emission from surface-bound RuC* on TiO_2 was considerably more quenched. In Figure 5e, the average emission lifetime of RuC-TiO_2 NPs was 279 ns in ACN solution, which is consistent with the emission quenching observation. As shown in Figure 5f, under visible illumination, excitation to produce RuC* on TiO_2 NPs is followed by the excited electron injection to the conduction band of TiO_2. The electron transfer from the excited-state RuC* to the conduction band (CB) of TiO_2 is energetically favorable. Upon electron transfer, the generated hole is on RuC.

$$TiO_2 - Ru(II)C \rightarrow TiO_2 - Ru(II)^*C \quad (2)$$

$$TiO_2 - Ru(II)^*C \rightarrow TiO_2(e^-) - Ru(III)C \quad (3)$$

These observations present clear evidence for energy/electron transfer between photoexcited RuC* and TiO_2 NPs (eq 2), resulting in charge separation and the formation of RuC(III) and TiO_2 (e^-) (eq 3). Thus, the RuC-TiO_2 NPs can facilitate light-induced charge separation, and the investigation next turned to assessing if the photoinduced electron−hole pairs could drive the photocatalytic cleavage of a lignin model compound under visible-light illumination.

The long-term photostability of RuC-TiO_2 NPs is critical to the use of this material for performing photocatalytic bond cleavage. Therefore, the long-term photostability of RuC-TiO_2 NPs was investigated in both aqueous and organic solvents. The RuC-TiO_2 NPs were dispersed in H_2O and ACN, and the colloidal RuC-TiO_2 NP solutions were irradiated under 2 sun illumination (200 mW·cm^{-2}) at room temperature over a period of 24 h. The RuC-TiO_2 NPs were then isolated by centrifugation, and the visible absorption spectrum of the supernatant solution was measured. As shown in Figure S3, the MLCT absorbance from RuC was observed in the H_2O supernatant solution, indicating desorption of RuC on TiO_2 due to hydrolysis of the Ti−O−C surface bonds between the anchoring moiety COOH and the TiO_2 surface.[39] In contrast, there were no apparent absorption features for RuC in the ACN supernatant solution. Under irradiation for 24 h, this confirmed the stability of RuC-TiO_2 NPs in a polar aprotic solvent, ACN. ACN was then chosen as a solvent for investigating photolytic bond cleavage of the lignin substrate.

Based on the above experiments, RuC-TiO_2 NPs can serve as a photocatalyst for $C_\alpha-C_\beta/C_\beta-O$ σ-bond cleavage in β-O-4 lignin model compounds under visible-light illumination and mild conditions. Our prior work had focused on phenolic lignin model compounds for the $C_{aryl}-C_\alpha$ bond cleavage with the oxidizing mediator ACT because the presence of a phenoxy group on the lignin substrate was important for realizing C−C bond cleavage.[15] This study is instead focused on investigating a nonphenolic lignin model compound, DMP-2ol, to obtain $C_\alpha-C_\beta/C_\beta-O$ σ-bond cleavage products at room temperature without the need of an additional mediator.

To carry out the photocatalytic conversion of DMP-2ol with RuC-TiO_2 NPs, DMP-2ol (4.13 mg, 0.0125 mmol) was dissolved in 5.0 mL of ACN with 8.8 mg/mL colloidal RuC-TiO_2 NP photocatalyst. The mixture was stirred continuously under 2 sun illumination (200 mW·cm^{-2}) at room temperature with the light passed through an AM 1.5G filter before the sample. Cleavage products **1** and **2** reaction were confirmed by ^1H and ^{13}C NMR analyses after the 24 h reaction (Figure S4). In addition, gas chromatography−mass spectrometry (GC−MS) analysis results confirmed that the structures of the two cleavage products **1** and **2** are consistent with the NMR data (Figure S5). DMSO was used as an internal standard in the ^1H NMR to determine the percent yield of the cleavage products 3,4-dimethoxybenzaldehyde (or veratraldehyde (V), **1**) and 2-methoxyphenol (or guaiacol (G′), **2**). The photocatalytic reaction with DMP-2ol in the RuC-TiO_2 NPs solution afforded the cleavage products **1** (82%) and **2** (90%) (Figure 6a). The $^1H-^{13}C$ heteronuclear single-quantum coherence (HSQC) NMR spectra clearly showed the consumption of DMP-2ol in the aliphatic region following a 24 h photocatalytic experiment (Figure 6b). The three major contours A_α (δ_C/δ_H 72.68/4.99), A_β (δ_C/δ_H 81.43/4.17), and A_γ (δ_C/δ_H 60.75/3.92, 3.67) of the starting DMP-2ol compound completely disappeared (Figure 6b, right). The disappearance of these three major peaks can be ascribed to C−O/C−C bond cleavage in DMP-2ol.[2,15,16] Simultaneously, as shown in Figure 6c in the aromatic region of the HSQC NMR, new chemical shifts appear after the photocatalytic cleavage reaction indicated by V_2 (at δ_C/δ_H 108.90/7.42), V_5 (at δ_C/δ_H 110.39/6.99), and V_6 (at δ_C/δ_H 126.88/7.47) for product **1** and G'_1 (at δ_C/δ_H 120.08/6.86), G'_2 (at δ_C/δ_H 110.65/6.86), G'_5 (at δ_C/δ_H 114.48/6.93), and G'_6 (at δ_C/δ_H 121.36/6.87) for product **2**. The HSQC NMR of product **1** shows a characteristic resonance for the aldehyde peak (δ_C/δ_H 190.9/9.87) (Figure 6c, right). These results indicate the formation of two major cleavage products. The HSQC NMR spectra were consistent with the above ^1H and ^{13}C NMR and GC−MS data. To confirm the influence of each component, control experiments without the photosensitizer RuC, TiO_2 NPs, or AM1.5G light illumination were performed, and the results are shown in Figure 6a. No products were observed either without RuC, TiO_2 NPs, or AM1.5G light illumination. This indicates that there is not a significant contribution from direct excitation of the TiO_2 NPs under the illumination conditions used. The photoexcitation of RuC on the surface of TiO_2 NPs is the key to trigger the visible-light-induced photocatalytic cleavage reaction in DMP-2ol due to the shift of the absorption edge to the visible region. Additionally, another common lignin

https://doi.org/10.1021/acsanm.1c03622
ACS Appl. Nano Mater. 2022, 5, 948−956

a)

	Yield (%)		
	DMP-2ol	1	2
Standard[a]	ND	82	90
No RuC	97	ND	ND
No TiO_2 NPs	97	< 3%	ND
No light	92	< 1%	ND

[a]0.25 mM DMP-diol in ACN with 8.8 mg/ml **RuC-TiO_2 NPs** under 200 mW/cm^2 solar irradiation for 24 hours.

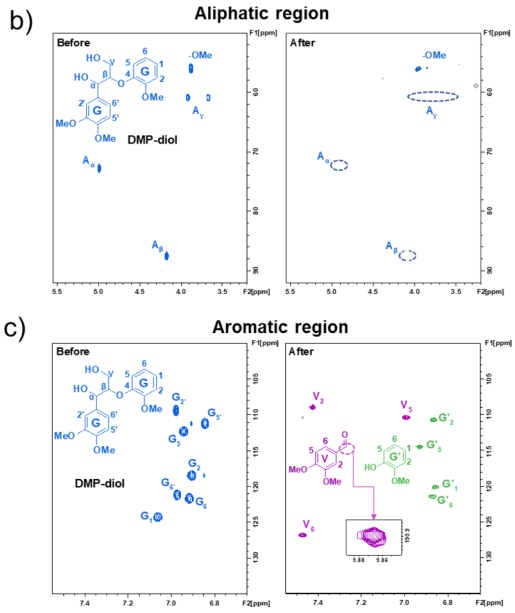

Figure 6. (a) Table of observed yields for cleavage products **1** and **2** over a 24 h reaction time with the indicated condition. $^{13}C-^{1}H$ HSQC NMR spectra of DMP-2ol before and after photocatalytic reactions under standard conditions by using RuC-TiO_2 NPs in (b) aliphatic and (c) aromatic regions.

model compound, 2-phenoxy-1-phenylethanol (PP-ol), which does not contain a 1° alcohol moiety or methoxy benzyl units, was tested with RuC-TiO_2 NPs under the same photocatalytic reaction conditions used for DMP-2ol. No C−C/C−O bond cleavage in the β-O-4 aryl ether linkage occurred, and an approximately 6% formation of the ketone form 2-phenoxy-1-phenylethanone from the starting PP-ol was observed over a 24 h experiment (Figure S6). The presence of 1° alcohol moieties and methoxy benzyl units would appear essential to achieving the cleavage reaction in the β-O-4 aryl ether linkage under the mild conditions studied here.

A proposed reaction mechanism for visible-light-driven selective cleavage of $C_\alpha-C_\beta/C_\beta-O$ σ-bonds in a nonphenolic compound with RuC-TiO_2 NPs is shown in Figure 7. The photoexcited RuC(II)* formed on TiO_2 NPs under visible illumination drives charge separation by electron injection to TiO_2 NP. After electron transfer from 2 equiv RuC(III) to DMP-2ol, the oxidized intermediate **3** is formed from DMP-2ol. Then, reduction of **3** by TiO_2 (e^-) or Ru(II)* generates a ketyl radical anion species[40] that undergoes $C_\beta-O$ σ-bond cleavage to produce the cleavage intermediates **4** and **5**.[41] Then, protonation and retroaldol $C_\alpha-C_\beta$ cleavage reaction affords fragmentation products **1** and **2**. It is noted that we were unable to observe the aldehyde in NMR. It could be possible that the acetaldehyde is removed during the evaporation process from the photocatalytic reaction mixture.

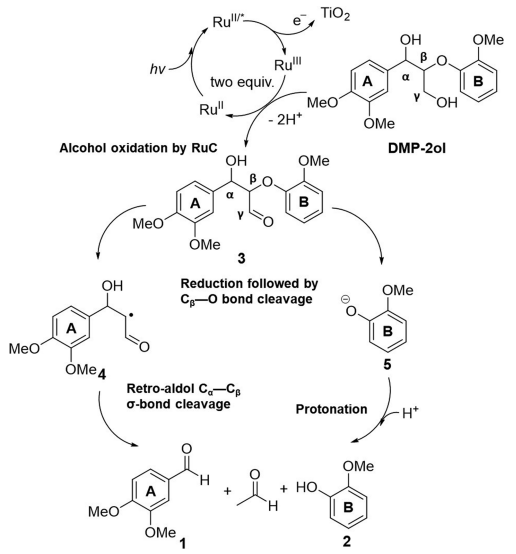

Figure 7. Proposed reaction mechanism for the chemoselective cleavage of $C_\alpha-C_\beta/C_\beta-O$ σ-bonds in a nonphenolic compound with RuC-TiO_2 NPs at room temperature.

The photostability and recyclability of the RuC-TiO_2 NPs are critical to the development of this photocatalytic method for solar-driven lignin valorization. The UV−Vis absorption of colloidal RuC-TiO_2 NPs solution in the presence of DMP-2ol was characterized both before and after the photocatalytic reactions. The MLCT absorption band from RuC in ACN was slightly reduced compared to the MLCT absorption band before the photocatalytic reaction (Figure 8a). We assume that proton sources from DMP-2ol could affect the hydrolysis of the Ti−O−C anchoring bonds between the moiety COOH and the TiO_2 surface. Figure 8b shows the recyclability of RuC−TiO_2 NPs by testing the conversion efficiency of the same sample over three consecutive experiments. The photocatalytic conversion efficiency for DMP-2ol to **1** and **2** over three independent reaction cycles was 90, 88, and 83%, respectively. A gradual loss in photocatalytic activity over the three cycles could arise from the hydrolysis of the interfacial RuC−TiO_2 NPs, leading to MLCT absorption loss. However, this system still maintained over 80% cleavage conversion of DMP-2ol over three cycles, indicating that the photocatalyst can be successfully recovered and recycled for further use without substantial loss in activity.

■ CONCLUSIONS

The RuC photocatalyst containing carboxylic acid-anchoring groups was successfully synthesized and immobilized on TiO_2 NPs. This RuC-TiO_2 NP system presents a facile method for achieving solar-light-driven cleavage of $C_\alpha-C_\beta/C_\beta-O$ σ-bonds in the β-O-4 aryl ether linkage of the DMP-2ol studied. Without the presence of additional oxidizing agents, the conversion of cleavage products was obtained in greater than 80% yield at room temperature. The photophysical properties of the RuC-TiO_2 NPs in the ACN solution were studied to better understand the photocatalytic process. The MLCT emission lifetime and quenching of RuC are influenced by the presence of TiO_2 NPs, indicating the intermolecular energy/electron transfer between the RuC and TiO_2 NPs. Furthermore, the optical band gap of the TiO_2 component from the RuC-TiO_2 NPs was similar to that of bare TiO_2 NPs.

https://doi.org/10.1021/acsanm.1c03622
ACS Appl. Nano Mater. 2022, 5, 948−956

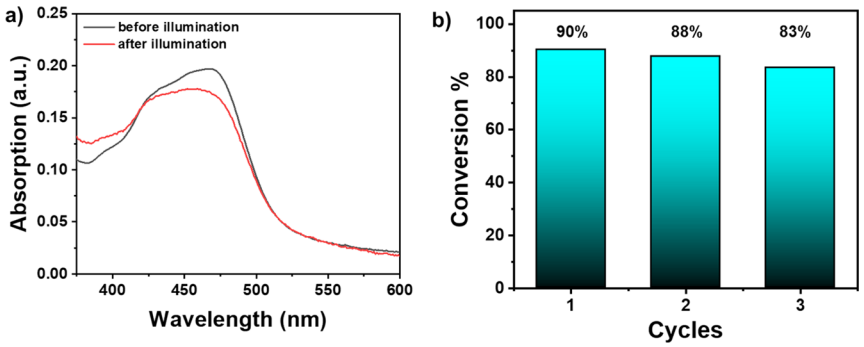

Figure 8. Photostability and recyclability of RuC-TiO_2 NPs with DMP-2ol for the solar-driven photocatalytic cleavage reaction at room temperature.

This indicates that the RuC complex did not influence the E_g of TiO_2 NPs. Based on intermolecular energy/electron transfer, the electron/hole pairs produced by photoexcited RuC-TiO_2 convert DMP-2ol to simple aromatic aldehyde (veratraldehyde) and phenolic (guaiacol) products with excellent yields. Further work with RuC-TiO_2 NPs will explore cleavage strategies in a wide range of lignin substrates and real lignin and attempt to elucidate the mechanistic path of the cleavage reaction at room temperature.

EXPERIMENTAL SECTION

Reagents. *cis*-Bis(2,2′-bipyridine)ruthenium(II) dichloride dihydrate, bromoacetophenone, phenol, potassium carbonate, sodium borohydride, and titanium(IV) isopropoxide were obtained from Sigma Aldrich and used without further purification. 2-Phenoxy-1-phenylethanol (PP-ol) was synthesized according to a previous report.[42] Bis(2,2′-bipyridine)(4,4′-dicarboxy-2,2′-bipyridine)Ru(II) (RuC) was synthesized as described previously.[43] 1-(3,4-Dimethoxyphenyl)-2-(2-methoxyphenoxy)propane-1,3-diol (DMP-2ol) was purchased from SY Innovation and used without further purification or modification. All the chemicals used for experiments were reagent-grade. An LSH-7320 ABA LED Solar Simulator purchased from ORIEL was used as the light source.

Preparation of TiO_2 NPs and RuC-TiO_2 NPs. *TiO_2 NPs.* TiO_2 NPs were synthesized according to a previous study.[44] Titanium(IV) isopropoxide (TIP) (20 g) was combined with isopropyl alcohol (IPA) (30 g), which was then mixed with tetrabutylammonium hydroxide (TBAOH) (4.6 g) combined with 76 mL of water. The TIP/IPA mixture was slowly added to the TBAOH/H_2O solution with vigorous stirring at room temperature. Subsequently, the mixed solution was boiled with continuous stirring for 2 h. The initially turbid, white colloidal suspension became a translucent and pale blue suspension. When the volume of the colloidal solution was reduced to 40 mL, an additional 40 mL of H_2O was added. The mixture was further heated until the volume was reduced to 45 mL of mixture solution. After the transparent colloidal TiO_2 suspension was cooled to room temperature, the mixture was transferred to a Teflon-lined autoclave, and the temperature was raised to 150 °C for 2.5 h. Then, the TiO_2 NPs were centrifuged out of the colloidal solution. The crude TiO_2 NPs were then washed with ethanol three times to remove the unreacted precursor. The TiO_2 NPs were dried in vacuo and stored in a sealed container at room temperature for further usage.

RuC-TiO_2 NPs. RuC was dissolved into acetonitrile (ACN) solvent (3 mg/mL) to prepare a stock solution. Then, TiO_2 NPs (1 mg/mL in acetonitrile) were mixed with the RuC solution (3 mg/mL in acetonitrile) in a 1:1 volume ratio and stirred for 24 h. The mixture was then centrifuged to obtain RuC-TiO_2 NPs. Purification by centrifugation and washing with methanol removed unbound RuC. The washing step was repeated three times to obtain the final RuC-TiO_2 NP construct. The obtained RuC-TiO_2 NPs were then dried in vacuo and stored at room temperature.

Photocatalytic Oxidative Cleavage of DMP-2ol. DMP-2ol (4.13 mg, 0.0125 mmol) was mixed with RuC-TiO_2 NPs (8.8 mg/mL) in acetonitrile solution followed by sonication with the mixture. Then, the solution was illuminated with 2 sun (200 mW·cm^{-2}) light passed through an AM1.5G filter for 24 h. The photocatalyst RuC-TiO_2 NPs were removed by centrifugation, and the supernatant was dried in vacuo for further characterizations.

Characterization Methods and Instrumentations. The reaction mixture was positioned to receive 200 mW·cm^{-2} for the solar simulation as determined by a S415C thermal power sensor head using a THORLABS PM400 optical power meter. Transmission electron microscopy (TEM, JEOL JEM-2100F) was operated at 200 kV. Powder X-ray diffraction of the nanoparticles was performed on a Bruker D2 Phaser with a LYKXEYE one-dimensional silicon strip detector using Cu K_α radiation (λ = 1.5406 Å).

UV−visible absorption spectra were obtained by using a Thermo Scientific Evolution 220 UV−Vis spectrometer. Emission spectra and fluorescence lifetime measurements were carried out using an Edinburgh FLS 980 steady-state and time-resolved emission spectrometer. The average emission lifetimes obtained from time-resolved photoluminescence measurements were calculated using the following equation

$$<\tau> = \frac{\sum_{i=1}^{2} \alpha_i \tau_i^2}{\sum_{i=1}^{2} \alpha_i \tau_i}$$

where $<\tau>$ is experimentally detected PL decay, α_i is the fractional amplitude of component i, and τ_i is the lifetime of component i.

The products were characterized by ^{1}H NMR and ^{13}C-NMR and Thermo Polaris Q Ion Trap Gas Chromatography/Mass Spectrometer (GC−MS). ^{1}H−^{13}C heteronuclear single-quantum coherence (HSQC) NMR was used for the structural analysis of lignin model compounds before and after the photocatalytic reaction. The analysis was conducted using a Bruker AVANCE III HD 800 MHz equipped with a TCI Cryo probe. The acquisition parameters were as follows: 12 ppm spectral width in F2 (1H) dimension with 1024 data points and 200 ppm spectral width in F1 (^{13}C) dimension with 512 data points, a 1.2 s pulse delay, and 32 scans. The ^{1}H−^{13}C HSQC experiment was conducted with a standard Bruker HSQC pulse sequence (hsqcetgpsis2), and the volume integration of contours in HSQC spectra was performed using Bruker TopSpin 4.0.6 software.

ASSOCIATED CONTENT

Supporting Information

The Supporting Information is available free of charge at https://pubs.acs.org/doi/10.1021/acsanm.1c03622.

(Figures S1−S6) TEM image and size distribution of TiO_2 NPs; UV−Vis absorption spectrum of RuC; illustration of RuC−TiO_2 NPs in H_2O and ACN; NMR spectra and GC−MS of products 1 and 2; ^{1}H NMR of PP-ol (PDF)

https://doi.org/10.1021/acsanm.1c03622
ACS Appl. Nano Mater. 2022, 5, 948−956

AUTHOR INFORMATION

Corresponding Author

Gyu Leem − *Department of Chemistry, State University of New York College of Environmental Science and Forestry, Syracuse, New York 13210, United States; The Michael M. Szwarc Polymer Research Institute, Syracuse, New York 13210, United States;* orcid.org/0000-0003-0169-1096; Email: gyleem@esf.edu

Authors

Shuya Li − *Department of Chemistry, State University of New York College of Environmental Science and Forestry, Syracuse, New York 13210, United States*

Udani K. Wijethunga − *Department of Chemistry, State University of New York College of Environmental Science and Forestry, Syracuse, New York 13210, United States*

Andrew H. Davis − *Department of Chemistry, Syracuse University, Syracuse, New York 13244, United States*

Saerona Kim − *Department of Chemistry, State University of New York College of Environmental Science and Forestry, Syracuse, New York 13210, United States*

Weiwei Zheng − *Department of Chemistry, Syracuse University, Syracuse, New York 13244, United States;* orcid.org/0000-0003-1394-1806

Benjamin D. Sherman − *Department of Chemistry & Biochemistry, Texas Christian University, Fort Worth, Texas 76129, United States;* orcid.org/0000-0001-9571-5065

Chang Geun Yoo − *Department of Chemical Engineering, State University of New York College of Environmental Science and Forestry, Syracuse, New York 13210, United States; The Michael M. Szwarc Polymer Research Institute, Syracuse, New York 13210, United States;* orcid.org/0000-0002-6179-2414

Complete contact information is available at: https://pubs.acs.org/10.1021/acsanm.1c03622

Author Contributions

#S.L. and U.K.W. contributed equally to this work.

Notes

The authors declare no competing financial interest.

ACKNOWLEDGMENTS

This work is supported in part by the USDA National Institute of Food and Agriculture, McIntire Stennis project (no. 1026335). W.Z. acknowledges support from the NSF CAREER grant (award no. CHE-1944978), NSF IUCRC Phase I grant (award no. 2052611), and Syracuse University CUSE Grant (SD-10-2020). B.D.S. thanks the Welch Foundation for support of this work through award no. P-2044-20200401.

REFERENCES

(1) Shi, S.-H.; Liang, Y.; Jiao, N. Electrochemical Oxidation Induced Selective C−C Bond Cleavage. *Chem. Rev.* **2021**, *121*, 485−505.

(2) Li, S.; Davis, K.; Leem, G. In Lignin Utilization Strategies: From Processing to Applications. *American Chemical Society* **2021**, *1377*, 97−121.

(3) Wang, M.; Lu, J.; Zhang, X.; Li, L.; Li, H.; Luo, N.; Wang, F. Two-Step, Catalytic C−C Bond Oxidative Cleavage Process Converts Lignin Models and Extracts to Aromatic Acids. *ACS Catal.* **2016**, *6*, 6086−6090.

(4) Yang, C.; Maldonado, S.; Stephenson, C. R. J. Electrocatalytic Lignin Oxidation. *ACS Catal.* **2021**, *11*, 10104−10114.

(5) Davis, K. A.; Yoo, S.; Shuler, E. W.; Sherman, B. D.; Lee, S.; Leem, G. Photocatalytic Hydrogen Evolution from Biomass Conversion. *Nano Converg.* **2021**, *8*, 6.

(6) Lancefield, C. S.; Ojo, O. S.; Tran, F.; Westwood, N. J. Isolation of Functionalized Phenolic Monomers through Selective Oxidation and C−O Bond Cleavage of the *β*-O-4 Linkages in Lignin. *Angew. Chem., Int. Ed.* **2015**, *54*, 258−262.

(7) Nguyen, J. D.; Matsuura, B. S.; Stephenson, C. R. J. A Photochemical Strategy for Lignin Degradation at Room Temperature. *J. Am. Chem. Soc.* **2014**, *136*, 1218−1221.

(8) Cui, T.; Ma, L.; Wang, S.; Ye, C.; Liang, X.; Zhang, Z.; Meng, G.; Zheng, L.; Hu, H.-S.; Zhang, J.; Duan, H.; Wang, D.; Li, Y. Atomically Dispersed Pt−N_3C_1 Sites Enabling Efficient and Selective Electrocatalytic C−C Bond Cleavage in Lignin Models under Ambient Conditions. *J. Am. Chem. Soc.* **2021**, *143*, 9429−9439.

(9) Han, G.; Yan, T.; Zhang, W.; Zhang, Y. C.; Lee, D. Y.; Cao, Z.; Sun, Y. Highly Selective Photocatalytic Valorization of Lignin Model Compounds Using Ultrathin Metal/CdS. *ACS Catal.* **2019**, *9*, 11341−11349.

(10) Liu, H.; Li, H.; Lu, J.; Zeng, S.; Wang, M.; Luo, N.; Xu, S.; Wang, F. Photocatalytic Cleavage of C−C Bond in Lignin Models under Visible Light on Mesoporous Graphitic Carbon Nitride through *π*−*π* Stacking Interaction. *ACS Catal.* **2018**, *8*, 4761−4771.

(11) Yoo, H.; Lee, M.-W.; Lee, S.; Lee, J.; Cho, S.; Lee, H.; Cha, H. G.; Kim, H. S. Enhancing Photocatalytic *β*-O-4 Bond Cleavage in Lignin Model Compounds by Silver-Exchanged Cadmium Sulfide. *ACS Catal.* **2020**, *10*, 8465−8475.

(12) Gazi, S.; Hung Ng, W. K.; Ganguly, R.; Putra Moeljadi, A. M.; Hirao, H.; Soo, H. S. Selective Photocatalytic C−C Bond Cleavage under Ambient Conditions with Earth Abundant Vanadium Complexes. *Chem. Sci.* **2015**, *6*, 7130−7142.

(13) Kärkäs, M. D.; Bosque, I.; Matsuura, B. S.; Stephenson, C. R. J. Photocatalytic Oxidation of Lignin Model Systems by Merging Visible-Light Photoredox and Palladium Catalysis. *Org. Lett.* **2016**, *18*, 5166−5169.

(14) Bosque, I.; Magallanes, G.; Rigoulet, M.; Kärkäs, M. D.; Stephenson, C. R. J. Redox Catalysis Facilitates Lignin Depolymerization. *ACS Cent. Sci.* **2017**, *3*, 621−628.

(15) Li, S.; Kim, S.; Davis, A. H.; Zhuang, J.; Shuler, E. W.; Willinger, D.; Lee, J.-J.; Zheng, W.; Sherman, B. D.; Yoo, C. G.; Leem, G. Photocatalytic Chemoselective C−C Bond Cleavage at Room Temperature in Dye-Sensitized Photoelectrochemical Cells. *ACS Catal.* **2021**, *11*, 3771−3781.

(16) Li, S.; Li, Z.-J.; Yu, H.; Sytu, M. R.; Wang, Y.; Beeri, D.; Zheng, W.; Sherman, B. D.; Yoo, C. G.; Leem, G. Solar-Driven Lignin Oxidation via Hydrogen Atom Transfer with a Dye-Sensitized TiO_2 Photoanode. *ACS Energy Lett.* **2020**, *5*, 777−784.

(17) Nair, V.; Dhar, P.; Vinu, R. Production of Phenolics via Photocatalysis of Ball Milled Lignin−TiO_2 Mixtures in Aqueous Suspension. *RSC Adv.* **2016**, *6*, 18204−18216.

(18) Kamwilaisak, K.; Wright, P. C. Investigating Laccase and Titanium Dioxide for Lignin Degradation. *Energy Fuels* **2012**, *26*, 2400−2406.

(19) Srisasiwimon, N.; Chuangchote, S.; Laosiripojana, N.; Sagawa, T. TiO_2/Lignin-Based Carbon Composited Photocatalysts for Enhanced Photocatalytic Conversion of Lignin to High Value Chemicals. *ACS Sustain. Chem.* **2018**, *6*, 13968−13976.

(20) Luo, N.; Wang, M.; Li, H.; Zhang, J.; Liu, H.; Wang, F. Photocatalytic Oxidation−Hydrogenolysis of Lignin *β*-O-4 Models via a Dual Light Wavelength Switching Strategy. *ACS Catal.* **2016**, *6*, 7716−7721.

(21) Ismael, M. Highly Effective Ruthenium-Doped TiO_2 Nanoparticles Photocatalyst for Visible-Light-Driven Photocatalytic Hydrogen Production. *New J. Chem.* **2019**, *43*, 9596−9605.

(22) Leem, G.; Sherman, B. D.; Schanze, K. S. Polymer-Based Chromophore−Catalyst Assemblies for Solar Energy Conversion. *Nano Converg.* **2017**, *4*, 37.

(23) Leem, G.; Keinan, S.; Jiang, J.; Chen, Z.; Pho, T.; Morseth, Z. A.; Hu, Z.; Puodziukynaite, E.; Fang, Z.; Papanikolas, J. M.; Reynolds,

J. R.; Schanze, K. S. $Ru(bpy)_3^{2+}$ Derivatized Polystyrenes Constructed by Nitroxide-Mediated Radical Polymerization. Relationship Between Polymer Chain Length, Structure and Photophysical Properties. *Polym. Chem.* **2015**, *6*, 8184−8193.
(24) Mottweiler, J.; Rinesch, T.; Besson, C.; Buendia, J.; Bolm, C. Iron-Catalysed Oxidative Cleavage of Lignin and β-O-4 Lignin Model Compounds with Peroxides in DMSO. *Green Chem.* **2015**, *17*, 5001−5008.
(25) Mitchell, L. J.; Moody, C. J. Solar Photochemical Oxidation of Alcohols using Catalytic Hydroquinone and Copper Nanoparticles under Oxygen: Oxidative Cleavage of Lignin Models. *Org. Chem.* **2014**, *79*, 11091−11100.
(26) Jiang, J.; Sherman, B. D.; Zhao, Y.; He, R.; Ghiviriga, I.; Alibabaei, L.; Meyer, T. J.; Leem, G.; Schanze, K. S. Polymer Chromophore-Catalyst Assembly for Solar Fuel Generation. *ACS Appl. Mater. Interfaces* **2017**, *9*, 19529−19534.
(27) Leem, G.; Sherman, B. D.; Burnett, A. J.; Morseth, Z. A.; Wee, K.-R.; Papanikolas, J. M.; Meyer, T. J.; Schanze, K. S. Light-Driven Water Oxidation Using Polyelectrolyte Layer-by-Layer Chromophore−Catalyst Assemblies. *ACS Energy Lett.* **2016**, *1*, 339−343.
(28) Leem, G.; Morseth, Z. A.; Wee, K.-R.; Jiang, J.; Brennaman, M. K.; Papanikolas, J. M.; Schanze, K. S. Polymer-Based Ruthenium(II) Polypyridyl Chromophores on TiO_2 for Solar Energy Conversion. *Chem. − Asian J.* **2016**, *11*, 1257−1267.
(29) Leem, G.; Morseth, Z. A.; Puodziukynaite, E.; Jiang, J.; Fang, Z.; Gilligan, A. T.; Reynolds, J. R.; Papanikolas, J. M.; Schanze, K. S. Light Harvesting and Charge Separation in a π-Conjugated Antenna Polymer Bound to TiO_2. *J. Phys. Chem. C* **2014**, *118*, 28535−28541.
(30) Hussain, M.; Ahmad, M.; Nisar, A.; Sun, H.; Karim, S.; Khan, M.; Khan, S. D.; Iqbal, M.; Hussain, S. Z. Enhanced Photocatalytic and Electrochemical Properties of Au Nanoparticles Supported TiO_2 Microspheres. *New J. Chem.* **2014**, *38*, 1424−1432.
(31) Kathiravan, A.; Renganathan, R. Photosensitization of Colloidal TiO_2 Nanoparticles with Phycocyanin Pigment. *J. Colloid Interface Sci.* **2009**, *335*, 196−202.
(32) Zhang, L.; Cole, J. M. Dye Aggregation in Dye-Sensitized Solar Cells. *J. Mater. Chem.* **2017**, *5*, 19541−19559.
(33) Venkatraman, V.; Yemene, A. E.; de Mello, J. Prediction of Absorption Spectrum Shifts in Dyes Adsorbed on Titania. *Sci. Rep.* **2019**, *9*, 16983.
(34) Lee, K. J.; Lee, Y. U.; Fages, F.; Ribierre, J.-C.; Wu, J. W.; D'Aléo, A. Blue-Shifting Intramolecular Charge Transfer Emission by Nonlocal Effect of Hyperbolic Metamaterials. *Nano Lett.* **2018**, *18*, 1476−1482.
(35) Makuła, P.; Pacia, M.; Macyk, W. How To Correctly Determine the Band Gap Energy of Modified Semiconductor Photocatalysts Based on UV−Vis Spectra. *J. Phys. Chem. Lett.* **2018**, *9*, 6814−6817.
(36) Medhi, R.; Marquez, M. D.; Lee, T. R. Visible-Light-Active Doped Metal Oxide Nanoparticles: Review of their Synthesis, Properties, and Applications. *ACS Appl. Nano Mater.* **2020**, *3*, 6156−6185.
(37) Sherman, B. D.; McMillan, N. K.; Willinger, D.; Leem, G. Sustainable Hydrogen Production from Water using Tandem Dye-Sensitized Photoelectrochemical Cells. *Nano Converg.* **2021**, *8*, 7.
(38) Shang, J.; Gao, X. Nanoparticle Counting: Towards Accurate Determination of the Molar Concentration. *Chem. Soc. Rev.* **2014**, *43*, 7267−7278.
(39) Hanson, K.; Brennaman, M. K.; Luo, H.; Glasson, C. R. K.; Concepcion, J. J.; Song, W.; Meyer, T. J. Photostability of Phosphonate-Derivatized, Ru^{II} Polypyridyl Complexes on Metal Oxide Surfaces. *ACS Appl. Mater. Interfaces* **2012**, *4*, 1462−1469.
(40) Hasegawa, E.; Takizawa, S.; Seida, T.; Yamaguchi, A.; Yamaguchi, N.; Chiba, N.; Takahashi, T.; Ikeda, H.; Akiyama, K. Photoinduced Electron-Transfer Systems Consisting of Electron-Donating Pyrenes or Anthracenes and Benzimidazolines for Reductive Transformation of Carbonyl Compounds. *Tetrahedron* **2006**, *62*, 6581−6588.
(41) Magallanes, G.; Kärkäs, M. D.; Bosque, I.; Lee, S.; Maldonado, S.; Stephenson, C. R. J. Selective C−O Bond Cleavage of Lignin Systems and Polymers Enabled by Sequential Palladium-Catalyzed Aerobic Oxidation and Visible-Light Photoredox Catalysis. *ACS Catal.* **2019**, *9*, 2252−2260.
(42) Sun, K.; Chen, S.; Zhang, J.; Lu, G.-P.; Cai, C. Cobalt Nanoparticles Embedded in N-Doped Porous Carbon Derived from Bimetallic Zeolitic Imidazolate Frameworks for One-Pot Selective Oxidative Depolymerization of Lignin. *ChemCatChem* **2019**, *11*, 1264−1271.
(43) Beer, P. D.; Szemes, F.; Balzani, V.; Salà, C. M.; Drew, M. G. B.; Dent, S. W.; Maestri, M. Anion Selective Recognition and Sensing by Novel Macrocyclic Transition Metal Receptor Systems. ^1H NMR, Electrochemical, and Photophysical Investigations. *J. Am. Chem. Soc.* **1997**, *119*, 11864−11875.
(44) Upamali, K. A. N.; Estrada, L. A.; De, P. K.; Cai, X.; Krause, J. A.; Neckers, D. C. Carbazole-Based Cyano-Stilbene Highly Fluorescent Microcrystals. *Langmuir* **2011**, *27*, 1573−1580.

https://doi.org/10.1021/acsanm.1c03622
ACS Appl. Nano Mater. 2022, 5, 948−956